Observations Of Turbulence In The Surf Zone

Ron George
R. E. Flick
R. T. Guza

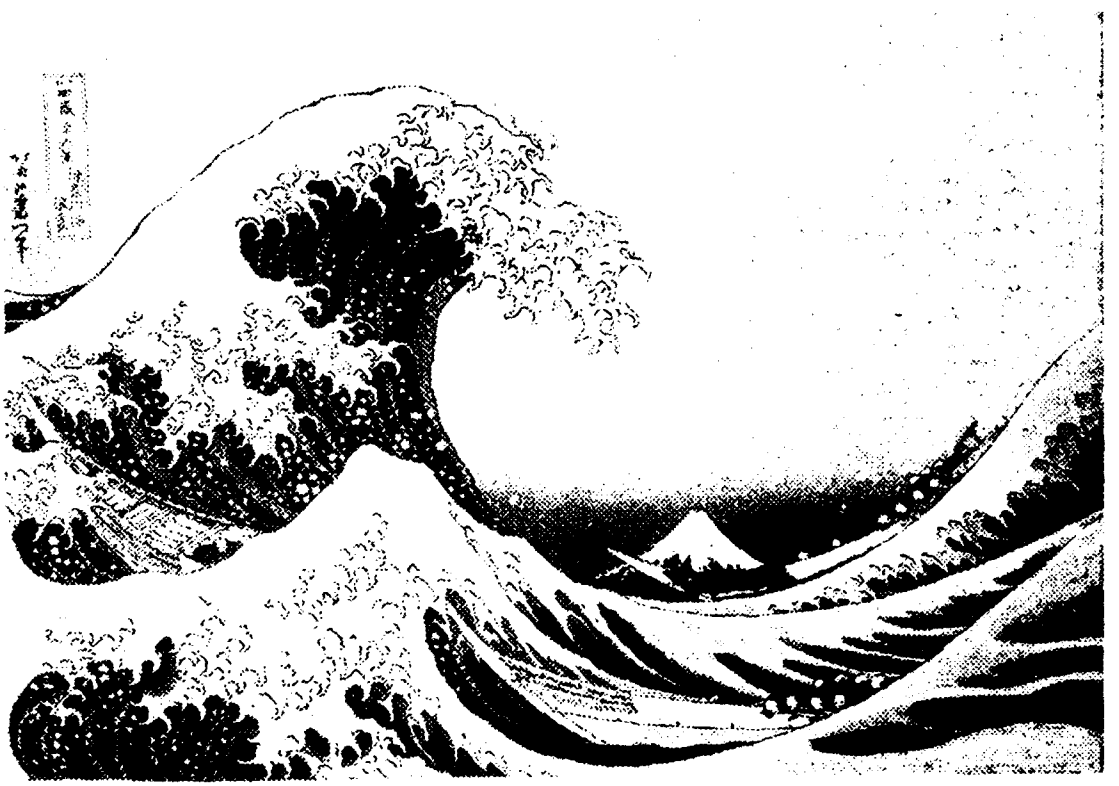

Center For Coastal Studies
Scripps Institution of Oceanography
University of California, San Diego

January 1993

SIO Reference Series No. 93-1

REPORT DOCUMENTATION PAGE

Form Approved
OMB No. 0704-0188

1. AGENCY USE ONLY (Leave blank)	2. REPORT DATE	3. REPORT TYPE AND DATES COVERED
	March 1993	Final 10/1/88-9/30/92

4. TITLE AND SUBTITLE
Nearshore Turbulence

5. FUNDING NUMBERS
N00014-89-J-1059

6. AUTHOR(S)
Reinhard E. Flick

7. PERFORMING ORGANIZATION NAME(S) AND ADDRESS(ES)
Scripps Institution of Oceanography, UCSD
Center for Coastal Studies, 0209
9500 Gilman Drive
La Jolla, CA 92093-0209

8. PERFORMING ORGANIZATION REPORT NUMBER

9. SPONSORING/MONITORING AGENCY NAME(S) AND ADDRESS(ES)
Office of Naval Research
Code 1121CS
800 North Quincy Street, Ballston Tower One
Arlington, VA 22217-5660

10. SPONSORING/MONITORING AGENCY REPORT NUMBER

11. SUPPLEMENTARY NOTES

12a. DISTRIBUTION/AVAILABILITY STATEMENT
No limitations

12b. DISTRIBUTION CODE

13. ABSTRACT (Maximum 200 words)

The turbulence generated by waves breaking on a natural beach is examined using hotfilm anemometer data. Turbulence intensity is estimated from the dissipation rate and an appropriate length scale (a fraction of the water depth). The dissipation rates are determined from wavenumber spectra found by applying Taylor's hypothesis to frequency spectra of short (1/8 s) hotfilm time series. The resulting Froude-scaled turbulence intensities are relatively uniform throughout the water column and are similar in vertical structure but lower in magnitude than in existing laboratory studies. The magnitures of the turbulence intensity observed in both the field and laboratory are consistent with an existing macroscopic model of bore dissipation in the surf zone. Scaling by this bore model relates turbulence intensity levels of monochromatic waves in small-scale laboratory experiments to random waves in the natural surf zone.

14. SUBJECT TERMS	15. NUMBER OF PAGES
Surfzone, Turbulence, Wave Breaking, Wave dissipation	34
	16. PRICE CODE

17. SECURITY CLASSIFICATION OF REPORT	18. SECURITY CLASSIFICATION OF THIS PAGE	19. SECURITY CLASSIFICATION OF ABSTRACT	20. LIMITATION OF ABSTRACT
Unclassified	Unclassified	Unclassified	SAR

Observations of Turbulence in the Surf Zone

Ron George
Center for Coastal Studies

R. E. Flick
California Department of Boating and Waterways

R. T. Guza
Center for Coastal Studies

Scripps Institution of Oceanography
University of California, San Diego

January 1993

SIO Reference Series No. 93-1

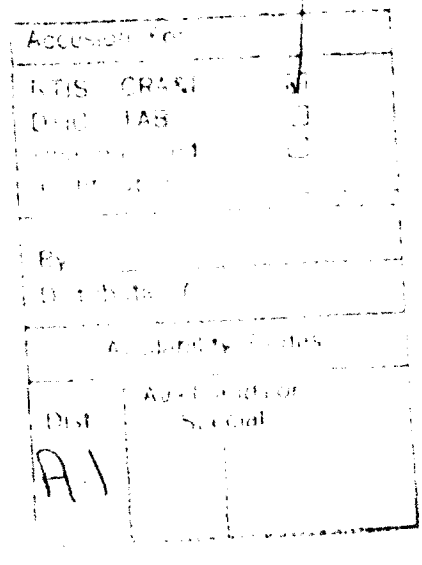

TABLE OF CONTENTS

ACKNOWLEDGEMENTS

This work was supported by the Office of Naval Research under grant #N00014-89-J-1059, by NOAA, National Sea Grant Program, Dept. of Commerce, under grant NA85AA-D-SG140, project R10E-3, and grant NA89AA-D-SG138, project R/CZ-90, through the California Sea Grant College Program, and by the California State Resources Agency. REF gratefully acknowledges support from the California Department of Boating and Waterways. Thanks to Bill Boyd and Mike Clifton for assistance with the field work, to Marcel Stive for generously sharing his laboratory data, and to Kazuo Nadaoka for helpful discussions.

ABSTRACT

The turbulence generated by waves breaking on a natural beach is examined using hotfilm anemometer data. Turbulence intensity is estimated from the dissipation rate and an appropriate length scale (a fraction of the water depth). The dissipation rates are determined from wavenumber spectra found by applying Taylor's hypothesis to frequency spectra of short (1/8 s) hotfilm time series. The resulting Froude-scaled turbulence intensities are relatively uniform throughout the water column and are similar in vertical structure but lower in magnitude than in existing laboratory studies. The magnitudes of the turbulence intensity observed in both the field and laboratory are consistent with an existing macroscopic model of bore dissipation in the surf zone. Scaling by this bore model relates turbulence intensity levels of monochromatic waves in small-scale laboratory experiments to random waves in the natural surf zone.

1. INTRODUCTION

Shoreward propagating sea and swell energy is transformed in the surf zone into motions of many different types and scales, including steady currents, low-frequency waves, organized vortical flows and high-Reynolds-number turbulence [Battjes, 1988]. Much attention has been devoted to the sea-swell and infragravity frequency bands (nominally 0.005 Hz to 0.5 Hz) because these motions dominate the sea-surface elevation and velocity spectra in typical natural surf zones. Less is known about higher frequency turbulent motions, which contain only a small fraction of the total kinetic energy of the nearshore velocity field, but usually dissipate most of the shoreward energy flux. Although many laboratory studies of surf zone turbulence have been conducted using breaking progressive waves [e.g., Nadaoka & Kondoh, 1982, Hattori and Aono, 1985, and Stive, 1980], hydraulic jumps [Resch and Leutheusser, 1972], and solitons [Skjelbreia, 1987], experiments in the natural surf zone have been hindered by instrumentation difficulties.

New measurements of turbulence intensity in the natural surf zone are described in Section 2. In Section 3, the wavenumber spectrum, $\Phi(\kappa)$, is obtained from a point measurement in this strongly oscillatory flow using Taylor's hypothesis (subject to a condition similar to Lin's [1953] criterion for the application of Taylor's hypothesis in *shear* flow). From the inertial subrange of $\Phi(\kappa)$ we estimate the dissipation rate ε and then the turbulence intensity using a form of the classical relationship $\varepsilon = u'^3/l$ where u' is the rms turbulence intensity and l is the energy-containing eddy scale. In Section 4 we

show that Froude-scaled surf zone turbulence levels are smaller in the natural surf zone than in existing laboratory studies. An existing model for the dissipation in a bore shows that the differences occur because the wave frequencies, wave-height to water-depth ratios, breaking intensities, and percentages of broken waves are substantially different. The turbulence levels observed in both the laboratory and field are consistent with the bore model.

2. EXPERIMENTS

Experiments were conducted at Scripps Beach, La Jolla, California during six days in March and April 1992 in water depths between 28 and 274 cm. This is a fine-grained gently sloping (about 1 in 40) sandy beach with relatively small alongshore depth changes. Waves broke by both spilling and plunging. Significant waveheights in 7 m water depth (a few hundred meters offshore) ranged from 50 to 120 cm.

Data were collected from three vertically separated hotfilm anemometers, two electromagnetic (EM) current meters with 4 cm spherical probes, one pressure sensor, and a videocamera recorder (VCR). The hotfilms were Thermo-Systems, Inc. (TSI) model 1755 constant-temperature anemometers with 1210-60W cylindrical quartz-coated platinum hotfilm probes. Although the most rugged of the cylindrical TSI probes, they are fragile. The more rugged conical 1230W probes have less desirable symmetry and gain characteristics. Relatively low operating temperatures (40 °C, producing an overheat ratio of roughly 8%) were used to avoid bubble formation on the probe.

All instruments except the VCR were mounted on a steel pipe frame (Figure 1) which was lowered daily by crane from Scripps pier and anchored to the sea bed 10 m up-drift (in the alongshore direction) from the pier. The hotfilms were located 40 cm up-drift from the EM current meters and the pressure sensor was buried about 10 cm in the sea bed. The VCR was used to determine the frequency and intensity of wave breaking. The time synchronization between the videocamera and the hotfilms was inadequate to determine which individual waves were broken. Anti-aliasing analog filters were applied to the hotfilm and current meter signals before digitization.

There were 70 data runs, each of 512-second duration. From the resulting potential 210 hotfilm time series, those with broken probes, instruments out of the water, or questionable calibrations were rejected, leaving 125 usable hotfilm time series. The vertical positions of the hotfilms are shown in Figure 2. While the broad wave height distribution produces no consistent "break point", breaking waves were infrequent deeper than h/H_o = 3.0.

Estimates of the aeration in the air bubble region (foam) on the leading face of a bore range from a few percent to as much as 40 percent [Fuhrboter, 1970]. The signal from a constant-temperature hotfilm anemometer is corrupted by the bubbles because air has much lower heat capacity than water. The bubble contamination was removed from the hotfilm signal, before calibration, as described in Appendix A.

Because of the difficulty of maintaining stable calibrations between the calibration facility and the ocean, the hotfilms were calibrated "in situ" using

EM current meters located at the same vertical elevation as the upper and lower hotfilm probes (See Appendix B). The mean of the EM current meter signals was used to calibrate the nearly equidistant middle hotfilm. Figure 3 shows time series of sea surface elevation and calibrated hotfilm speeds for cases in which most (panels a-d) and few (panels e-g) waves were broken. The increase in high-frequency velocity fluctuations from outside to inside the surf zone (compare panels g and c) is much larger than the corresponding increase in wave height and orbital speeds (compare e and f with a and b), suggesting that breaking waves (not vortex shedding or vibration of the instruments) generate the high frequency fluctuations.

3. RESULTS

Methods of Estimating Turbulence Intensity

Turbulence in steady free-stream flow or towed-body experiments is often defined as the fluctuation about the mean velocity [e.g., Hinze, 1976]. In a laboratory surf zone with monochromatic plane waves, turbulence has been defined as the deviation from an ensemble average of velocities at the same wave phase [Flick, Guza, and Inman, 1981]. The stochastic nature of natural orbital wave velocities precludes use of this definition.

Thornton [1979] separated surf zone orbital wave energy from turbulence by defining the wave orbital motions as the velocity fluctuations coherent with the sea surface elevation and assuming that all incoherent velocities are turbulence. However, this definition does not include as turbulence the largest scale eddies which do, in fact, influence the sea surface

[Nadaoka, Hino, and Koyano, 1989]. These large eddies may contribute significantly to the Reynold's stresses. Further disadvantages are that nonlinearity [e.g. Flick, Guza, and Inman, 1981] and directional spreading [Herbers, Lowe, and Guza, 1991] in a non-turbulent wave field also reduce the coherence between sea surface elevation and velocity. While the relative underestimation of the more energetic orbital flow is small, overestimation of the relatively low turbulent energy levels may be large.

The hotfilm frequency spectra (Figure 4) typically exhibit distinct turbulent (expected inertial subrange slope is $f^{-5/3}$) and orbital wave (expected spectral slope is f^{-3}, [Thornton, 1979]) regimes. However, the transition (where the slope changes) between the two regimes indicates only where dominance changes, not the low-frequency end of the turbulent inertial range. There is an overlap of unknown extent, which prevents accurate estimation of turbulence intensity by high-pass filtering above a single "cutoff frequency" [Nadaoka and Kondoh, 1982]. Because the coherence and cutoff methods are inaccurate, we calculate the turbulence intensity from the dissipation rate as described below.

Taylor's Hypothesis

The dissipation rate, ε, of a one-dimensional wavenumber spectrum $\Phi(\kappa)$ may be found from the universal form of the inertial subrange

$$\phi(\kappa) = \alpha \epsilon^{2/3} \kappa^{-5/3} \qquad (1)$$

where κ is the wavenumber magnitude and α (nominally 0.5) is the one-dimensional Kolmogorov constant. We first estimate $\Phi(\kappa)$ from the measured frequency spectrum $\Phi(f)$.

Laboratory experiments commonly concern relatively weak turbulence intensity (u′) in a spatially and temporally steady advective flow (U);

$$U > u'. \tag{2}$$

In this case Taylor's hypothesis can be used to convert the entire frequency spectrum (from time series measured at a fixed point) to the desired wavenumber spectrum:

$$\phi(\kappa) = \frac{\phi(f)}{2\pi/U} \tag{3}$$

where

$$\kappa = \frac{2\pi f}{U}. \tag{4}$$

When applied in situations with an unsteady advective flow field, U signifies all non-turbulent flow: orbital wave, lower frequency, and mean. Because the orbital wave velocities that dominate the nearshore spectrum change over a wave period, we use 1/8 s sections of the 512 s records and choose only those where (2) is satisfied. To verify (2), u′ was crudely estimated by high-pass filtering the full 512 s time series at f_o, approximately the transition between

the orbital-wave and turbulent inertial regimes. Using the definition $f_c = U/l \sim (g/h)^{1/2}$, ($l \approx h$ is the energetic eddy scale and $U = (gh)^{1/2}$ is a common surf zone scaling velocity), f_c fell near the slope break in the velocity spectrum (e.g. Figure 4).

Changes in the wave-dominated flow field during the 1/8 s records will also distort the f-κ transformation (4). Lin [1953] considered a similar type of distortion in strong shear flows and suggested that Taylor's hypothesis may be applied to the high wavenumber turbulent flow fluctuations only if the nonuniformity of the convection velocity over the eddy size is small compared to the convection velocity itself:

$$\kappa > \frac{2\pi dU/dz}{U}, \tag{5}$$

where z is the vertical (transverse) axis. The temporal unsteadiness in the present case is analogous to the spatial shear. We modify Lin's criterion (5), for use in unsteady flow, to simply

$$U > \Delta U, \tag{6}$$

where ΔU is the magnitude of the change, over the 1/8 s record, of the low-pass filtered cross-shore velocity U.

One further criterion, unrelated to Taylor's hypothesis, insures that only the u component of the turbulent velocity is used in the dissipation rate

estimate. (u, v, and w denote flow components in the cross-shore, longshore, and vertical directions, respectively.) This criterion (see Appendix C),

$$U \gg V,W \tag{7}$$

is necessary because the hotfilm probe senses flow from all directions. We have no independent measure of W, the low-frequency vertical flow, but expect that U >> W for long waves in the shallow waters of the nearshore.

U, V and ΔU were estimated for each 1/8 s data segment, and u'(t) was estimated for each 512 s data segment as described above. When a 1/8 s data segment did not satisfy all criteria (Equations 2,6, and 7), the 1/8 s data "window" was moved in increments of 1/32 s through the data until the next usable section was found. The >> factor for all criteria was chosen as 5. Varying the factor from 4 to 7 typically produced 10% variation in the resulting u' estimate. About 45% of the data passed all criteria, with extremes of 5% and 65% for individual 512 second records.

Dissipation Rate

Each selected 1/8 s data segment was detrended, a frequency spectrum calculated, and a wavenumber spectrum found from (3) and (4). A dissipation rate was calculated by applying (1) to the best fit $\kappa^{5/3}$ line through the wavenumber spectrum. (Perhaps because of the short time series, there were wide range of spectral slopes. The mean for all 1/8 s pieces was -1.25, less than the expected -5/3, possibly owing to the effect of bubbles on the dissipation rate [Wang, 1985].)

A plausible next step would be to average the 1/8 second ε values within each 512 s record. However, ε in the natural surf zone is highly intermittent (e.g., Figure 3(c)) and Oboukhov [1962] suggested that intermittency in otherwise homogeneous turbulence produces an approximately lognormal distribution of dissipation rate. The expected value, $\langle\varepsilon\rangle$, of a lognormally distributed dissipation rate does not equal the mean, mode, or median ε, as it would for a normally distributed variable. If ε is a lognormally distributed random variable, e.g., $Z=\ln\varepsilon$ is normally distributed, then

$$\langle\varepsilon\rangle = (\mu + \sigma^2_{\ln\varepsilon}/2) \tag{8}$$

where μ and $\sigma^2_{\ln\varepsilon}$ are the mean and variance of Z. Surf zone dissipation rates are generally lognormally distributed and the sample sizes small, so a graphical procedure [Baker and Gibson, 1987, see Figure 5] was used to estimate μ and $\sigma^2_{\ln\varepsilon}$ and thus $\langle\varepsilon\rangle$ for each 512 s data segment. Uncertainty in the resulting $\langle\varepsilon\rangle$ introduced by the estimation process produces uncertainty in the turbulence intensities ranging from ±3% to ±15%, with a mean of ±5%. Record lengths of 1/16 and 1/4 s produced turbulence intensities within ±10% of the 1/8 s values.

Kolmogorov [1962] defined $\sigma^2_{\ln\varepsilon}$ as the intermittency. Natural surf zone intermittencies ranged from about 2 to 12, with most values falling between 3 and 8, while deep ocean values ranged from 3 to 7 [Baker and Gibson, 1987]. The highest intermittencies occurred where very few waves were broken.

Dissipation rates (from the graphical procedure) for 512 s records in the natural surf zone ranged from 0.5 to 500 cm^2/s^3. Dissipation rates in 100 cm water depth were typically of order 100 cm^2/s^3, compared to 10^{-3} to 10^{-2} cm^2/s^3 in the equatorial undercurrent [Crawford and Osborne, 1980] and 10^{-2} to 1 cm^2/s^3 in the tidal channel observed by Grant, Stewart, and Moilliet, [1962].

Figure 6 shows normalized dissipation rates in and outside of the surf zone. Dissipation rates within the surf zone were generally much larger than seaward of the surf zone. There is a weak dependence of the dissipation rate on h/H_0 within the surf zone.

Dissipation rates also were calculated using (1) applied to wavenumber spectra produced by applying Taylor's hypothesis to the frequency spectra of 512 s runs with U equal to the r.m.s. orbital velocity [Lumley and Terray, 1983]. This is a crude approximation because the criteria for Taylor's hypothesis are sometimes grossly violated. Dissipation rates were also calculated by integrating the dissipation spectrum, formed from the 512 s wavenumber spectrum, over the approximate inertial and viscous subranges [Hinze, 1976]. Both methods provided dissipation rates within roughly a factor of two of the $\langle\varepsilon\rangle$ values calculated from the 1/8 s records with the graphical procedure.

Turbulence Intensity

Turbulence intensity, u', was estimated from the dissipation rate, $\langle\varepsilon\rangle$, using

$$u' = (\int_{\kappa_0}^{\infty} \phi(\kappa)\delta\kappa)^{1/2} \tag{9}$$

where $\Phi(\kappa)$ is defined by (1), giving

$$u' = (\frac{3}{2}\alpha)^{1/2}(\frac{\epsilon}{\kappa_0})^{1/3}. \tag{10}$$

Svendsen [1987] suggested that the turbulent length scale $l=2\pi/\kappa_0$ is between 0.2h and 0.3h. We used l = 0.25h (note the weak sensitivity of u' to the exact value of l), except for sensors closer to the bed than 0.25h that were influenced by the bottom boundary layer (i.e., $<\varepsilon>$ at the bottom sensor was larger than $<\varepsilon>$ at the middle sensor), in which case l was set equal to the distance to the bed.

For three-dimensional turbulence, the inertial dissipation estimator used is consistent with Gibson's [1990] definition of turbulence; the inertial vortical forces are larger than the damping forces because buoyancy forces in the surf zone are small relative to the inertial vortex forces. However, the inertial dissipation method does not include as turbulence the large two-dimensional eddies and "eddy-like flow" [Nadaoka, Hino, and Koyano, 1989] because they are not dissipative. These flows may contribute substantially to the Reynold's stresses.

Figure 7(a) shows that the normalized turbulence intensities within the surf zone ($h/H_0 < 3.0$) are roughly 10% of the orbital wave velocities.

Turbulence intensities are smallest near the bed and slowly increase over the water column, consistent with strong mixing of turbulence from the surface downward.

Turbulence intensities were also estimated from the coherence between sea-surface elevation and cross-shore orbital velocity. They were generally greater than 30% of orbital wave velocities (compared to 10% by the dissipation method) and independent of fraction of broken waves. The directional spread of the sea-swell wave field reduces the coherence and severely biases the estimate of u'.

Turbulence intensities were compared to a model, based on the energy balance in a hydraulic jump, which yields a depth-averaged dissipation rate [Thornton and Guza, 1983],

$$<\epsilon>=\frac{1}{4}\rho g\gamma^3 hfB^3 \tag{11}$$

where f is the wave frequency, γ is the wave-height to water-depth ratio, and B is a breaker coefficient related to the intensity of wave breaking. Combining (10) and (11), using $\kappa_0 = 2\pi/(0.25h)$, and following Thornton and Guza [1983],

$$u'_{\epsilon} = \gamma B(\frac{3}{8}\alpha)^{1/2}(\frac{fw_b}{4\pi}\rho g h^2)^{1/3} \tag{12}$$

where w_b is the fraction of broken waves. B and w_b were determined from the videocamera records for each 512 s data run. Past estimates of B, found by

fitting the observed wave height decay across both lab and field surf zones to model predictions based on (11), are about 1.0 [Thornton and Guza, 1983]. However, the precise relationship of B to breaking wave properties is unknown. We estimated B as the fraction of the bore face that is foam-covered; the range was roughly 0.4 to 0.9 with a mean value for all data of 0.7. The broken-wave fractions varied from less than 0.1 to near 1.0 and the wave-height to water-depth ratio, γ, varied from 0.2 to 0.6.

The ratio u'/u'_ϵ is surprisingly close to 1 (Figure 7(b)), considering that (11) provides only a rough estimate of the dissipation rate. The mean deviation (over the vertical) of u'/u'_ϵ from 1.0 is about +.05, less than the scatter in the estimates themselves at a given vertical position. Turbulence intensities were also Froude scaled (i.e., normalized by $(gh)^{1/2}$, [Svendsen, 1987]) in Figure 7(c) for comparison with laboratory data in the following section.

4. COMPARISON TO LABORATORY RESULTS

The present results are are compared to previous laboratory studies by Stive [1980] and Hattori and Aono [1985] (H & A) in Figure 8, where u′ is Froude scaled. While the weak dependence on vertical position is similar in the field and laboratory profiles, the scaled field turbulence intensity is less than 1/2 of the laboratory values.

These laboratory studies used monochromatic and unidirectional waves, each of which breaks with about the same intensity. However, naturally occuring waves are stochastic with a mix of unbroken and broken waves of

various heights and frequencies. These complexities are heuristically included in the bore-model based estimates of turbulence intensity (Figure 7b). The bore model can also be applied to monochromatic waves by setting both the breaker coefficient and broken-wave fraction equal to 1.0 and using observed values of γ. This scaling collapses the u′ values from lab and field to within a factor of two (Figure 9), an improvement over Froude scaling (Figure 8). The mean deviation (over the vertical) of u'/u'_c from unity is about +0.35 for Stive's results and -0.20 for Hattori and Aono, compared to +0.05 for the field data, (Figure 9(a)).

Stive separated turbulent and wave motions by ensemble phase averaging which probably slightly overestimates the turbulence intensity because of irregularities unrelated to turbulence in paddle-generated waves [Svendsen, 1987]. This is consistent with $u'/u'_c > 1$ as observed for the Stive data (Figure 9a).

The bore-model estimates of u'_c for Hattori and Aono may be biased low because their data were taken over a flat bed shoreward of a 1/20 beach slope which extended from deep water to near the break point. In their experiment, γ decreased from roughly 0.8 near the break point to 0.4 as the bores progressed shoreward (this variation was included in (12)). It is possible that B also decreased, but B was assumed 1.0 in (12). H & A estimated u′ with sea-surface elevation coherence. In a laboratory wave channel where directional spreading is probably unimportant, the method may underestimate u′ by not including the largest eddies as turbulence. Overestimates of B and underestimates of u′ would both tend to give $u'/u'_c < 1$ as observed (Figure

9b). Nadaoka and Kondoh's [1982] results (not shown) were biased very low, (about 30% of u'_e), consistent with their expectations that the high-pass filter method used to separate turbulence from orbital velocities introduces large errors.

5. CONCLUSIONS

Turbulence intensities in the natural surf zone were estimated using dissipation rates and a characteristic eddy length scale equal to 1/4 of the water depth. The dissipation rates were determined from wavenumber spectra found by applying Taylor's hypothesis to frequency spectra of 1/8 s hotfilm time series. The dissipation rates were intermittent, requiring lognormal statistics to determine expected values. The measurements show that surf zone turbulence intensities are smallest near the sea floor and slowly increase over the water column, consistent with strong mixing from the surface downward. The turbulence intensities agree very well with predictions from a macroscopic bore dissipation model which includes the effects of variations in wave frequency, broken-wave fraction, breaker coefficient, and wave-height to water-depth ratio. Good agreement was also found between field and laboratory turbulence intensities when normalized by the bore model. The large ratios of field-to-laboratory wave heights (e.g., 30:1) and frequencies (e.g., 10:1) indicate that bore-model scaling of surf zone turbulence intensity is robust over large differences in scale.

6. APPENDICES

A. Bubbles

The signal from a constant-temperature hotfilm anemometer is corrupted by bubbles because air has much lower heat capacity than water. The hotfilm power (and therefore output voltage) required to maintain constant temperature is much smaller in air than in water at the same velocity, [Delhaye, 1969]. The hotfilm output voltage signal during the passage of an air bubble is characterized by a steep-sided trough (Figure A). Resch, Leutheusser, and Alemu [1974], studying turbulence levels in a hydraulic jump, used dropout voltage, the distance between the local signal maximum in the water and the minimum in the bubble, to recognize bubbles. However, there is no consistent dropout voltage in the surf zone due to widely varying bubble sizes and advective velocities, so we used a slope threshold method from Wang [1985]. The maximum slope of the signal dropout is steeper than voltage changes associated with flow fluctuations. The hotfilms were sampled at 2048 Hz for bubble removal. Once recognized, each bubble signal was replaced using linear interpolation and the time series reduced by block-averaging to 64 Hz.

B. Calibration

The electromagnetic current meters (calibrated in a laboratory flow channel with accuracy of a few cm/s; see Guza, Clifton, and Rezvani, [1988]) were used to calibrate the hotfilms in situ. Both the hotfilm voltage, which is inherently rectified because the probe senses only the velocity magnitude, and

the absolute value of the EM current meter cross-shore velocity were reduced to 8 Hz. To reduce temporal lag problems caused by the small distance separating the hotfilm and EM current meter, the data points in each of the two time series was independently ranked according to magnitude and then recoupled so that each hotfilm voltage was paired with the EM speed of the same rank. The data pairs were then averaged for bins spanning 5 cm/s. A log-log polynomial provided an acceptable and convenient fit to the resulting paired data. Each 512 s hotfilm time series was independently calibrated and plotted (Figure B(1)). Time series with obviously bad fits were discarded. The
EM and calibrated hotfilm time series were similar at sea-swell frequencies (Figure B(2)).

C. Binomial Expansion of Hotfilm Signal

A hotfilm probe senses and rectifies flow from all directions, giving a signal of

$$S(t)=(u^2+v^2+w^2)^{1/2}$$

where u = U + u'. If U>>u' and U>>V,W then

$$S(t)=((U+u')^2+v'^2+w'^2)^{1/2}$$

so that

$$S(t) = (U^2 + 2Uu' + O(u'^2))^{1/2} = U + u' + O(u'^2).$$

7. FIGURES

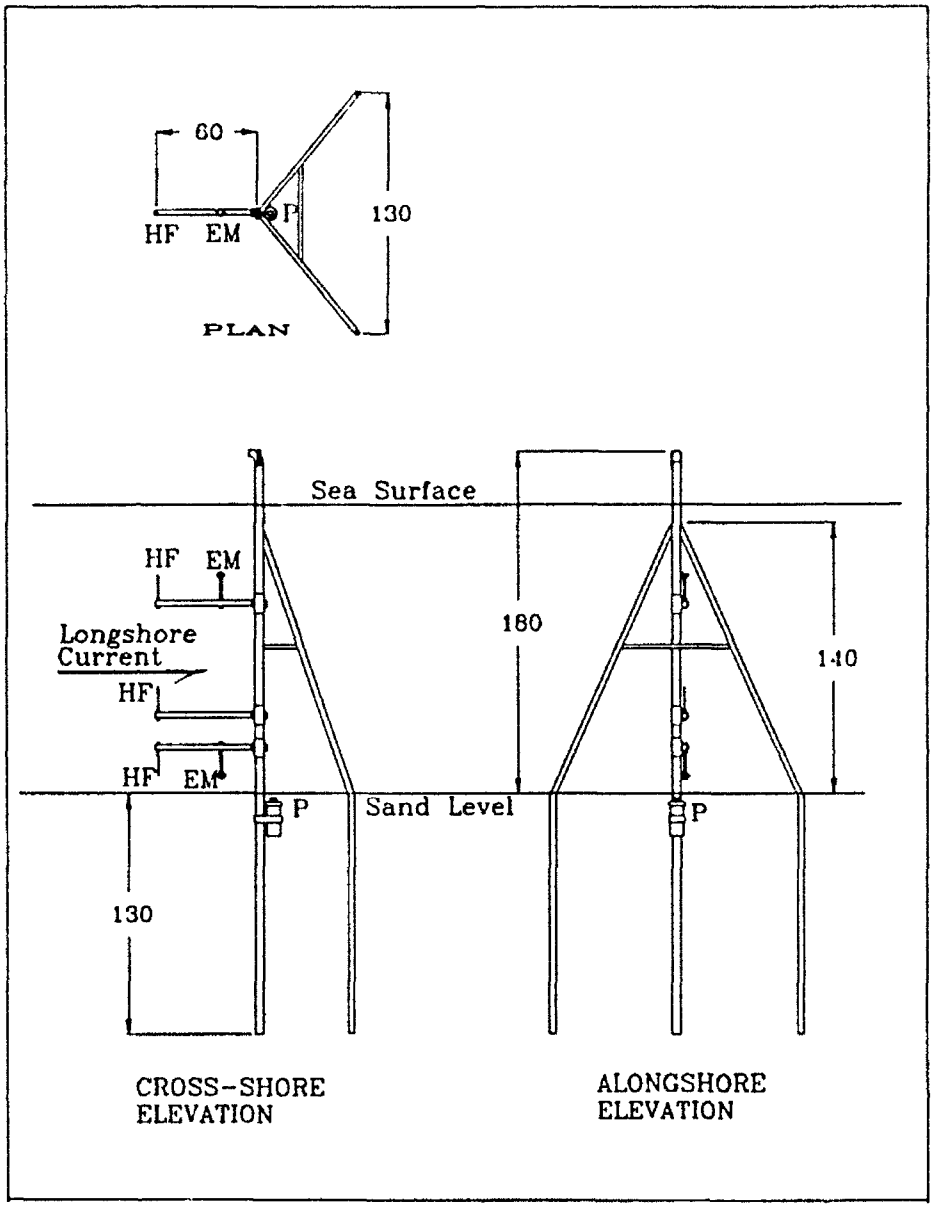

Figure 1. Instrument package mounting frame with positions of hotfilms (HF), electromagnetic current meters (EM), and pressure sensor (P). Dimensions are in cm. (a) Plan view. (b) View looking cross-shore. (c) View looking alongshore.

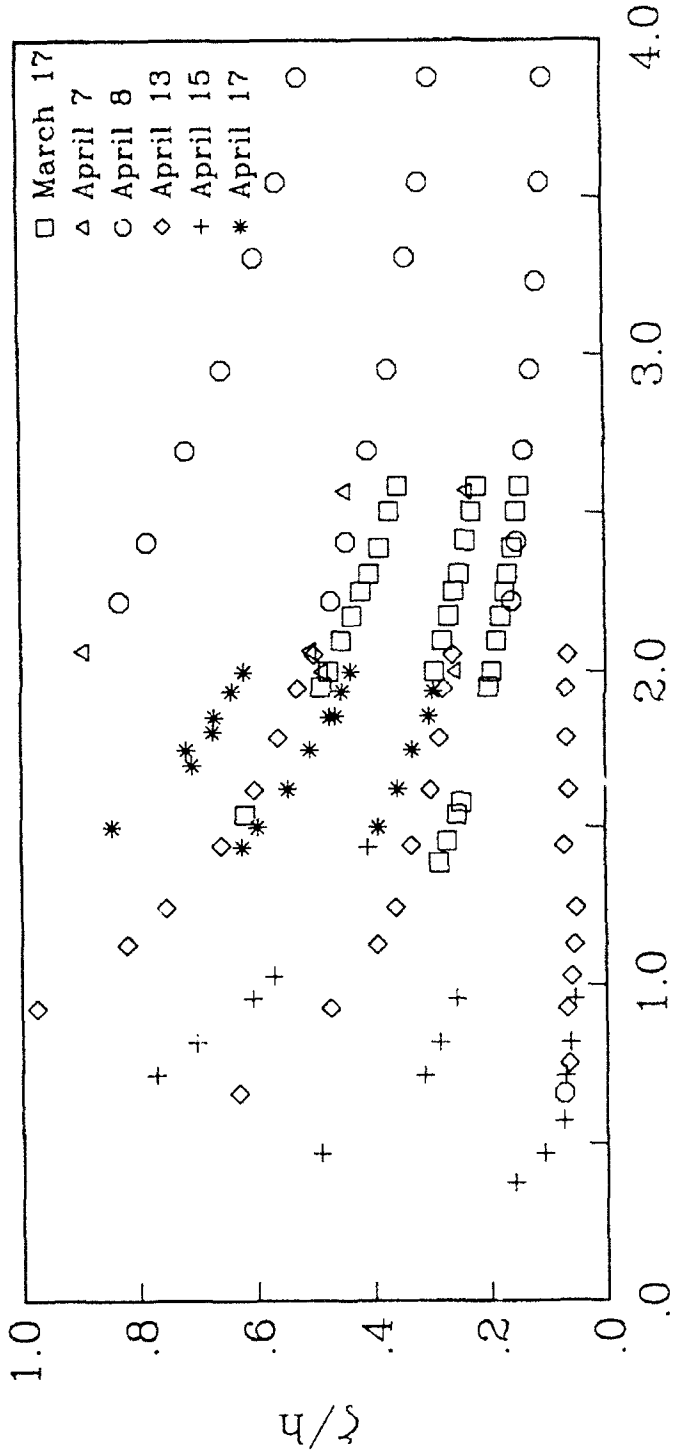

Figure 2. Relative vertical position of hotfilm probes vs normalized depth. ζ is elevation of the hotfilm above the bed, h is water depth and H_0 is the significant waveheight in 7 m depth.

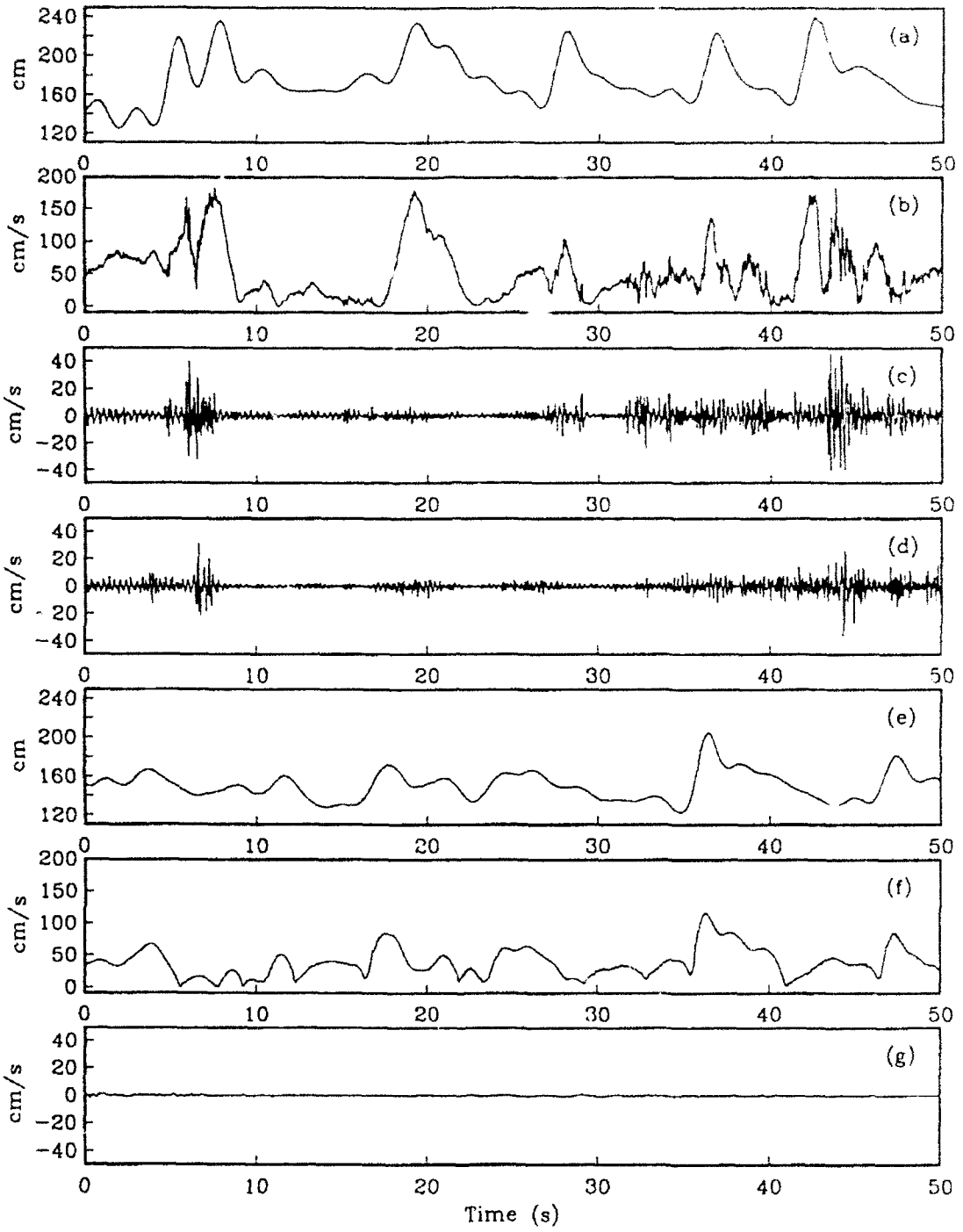

Figure 3. Representative time series: (a-d) In surf zone; 60% of waves broken; h=178cm; γ=H/h=0.33. (a) Sea surface elevation from the pressure data and linear theory. (b) Hotfilm speed. (c&d) Hotfilm high-pass filtered at f_c=2.35 Hz, (c) Elevation above bed: ζ=119 cm. (d) ζ=84 cm. (e-g) Seaward of surf zone; 3% of waves broken; h=149 cm; γ=H/h=0.28; ζ=119 cm. (e) Sea surface elevation. (f) Hotfilm speed. (g) Hotfilm high-pass filtered at f_c.

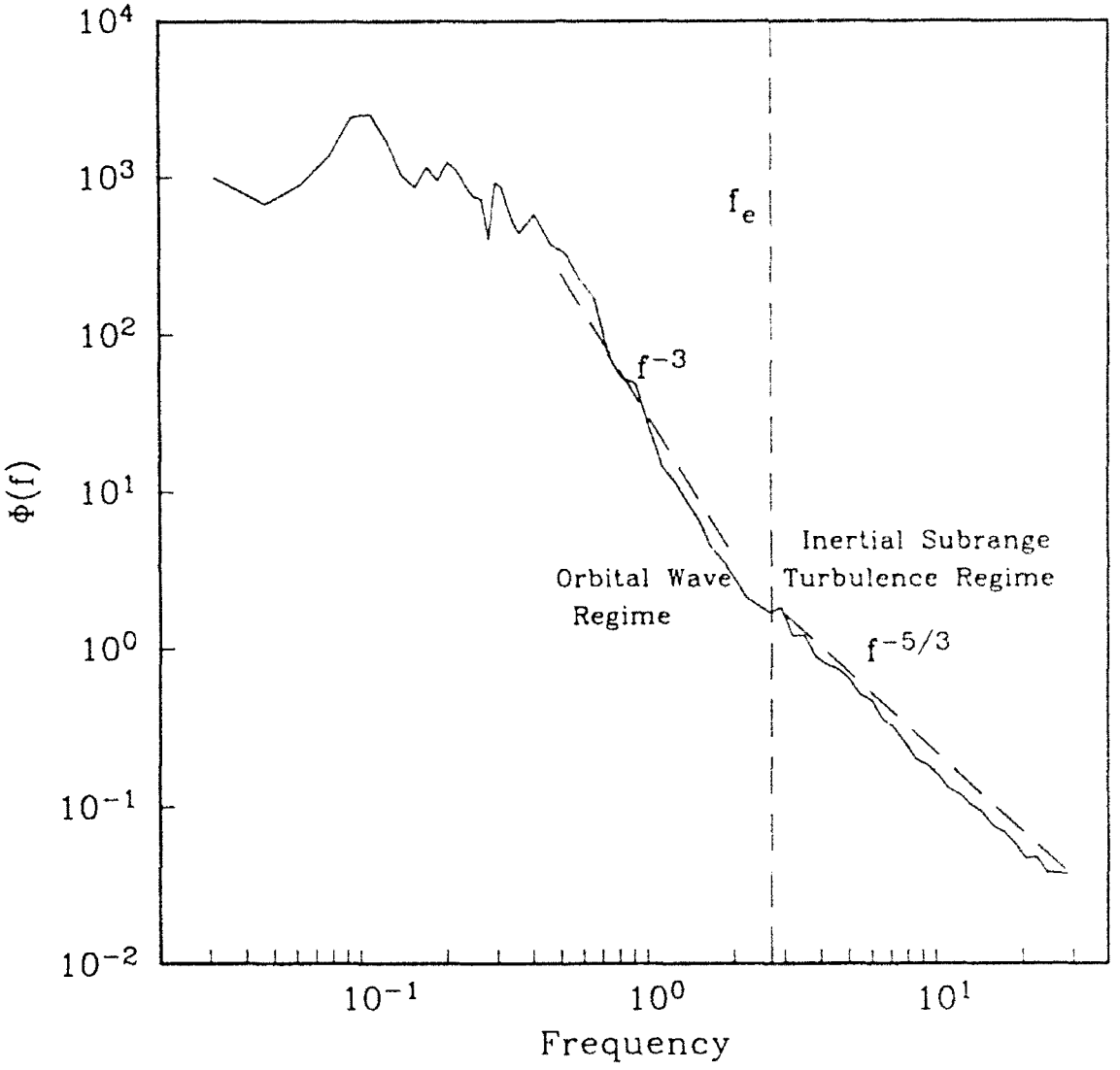

Figure 4. Frequency spectrum of a typical 512 s hotfilm time series, showing orbital wave (f^{-3} slope) and inertial subrange turbulent ($f^{5/3}$ slope) regimes. h=134 cm; ζ/h=0.29; DOF increases with frequency from 62-11000.

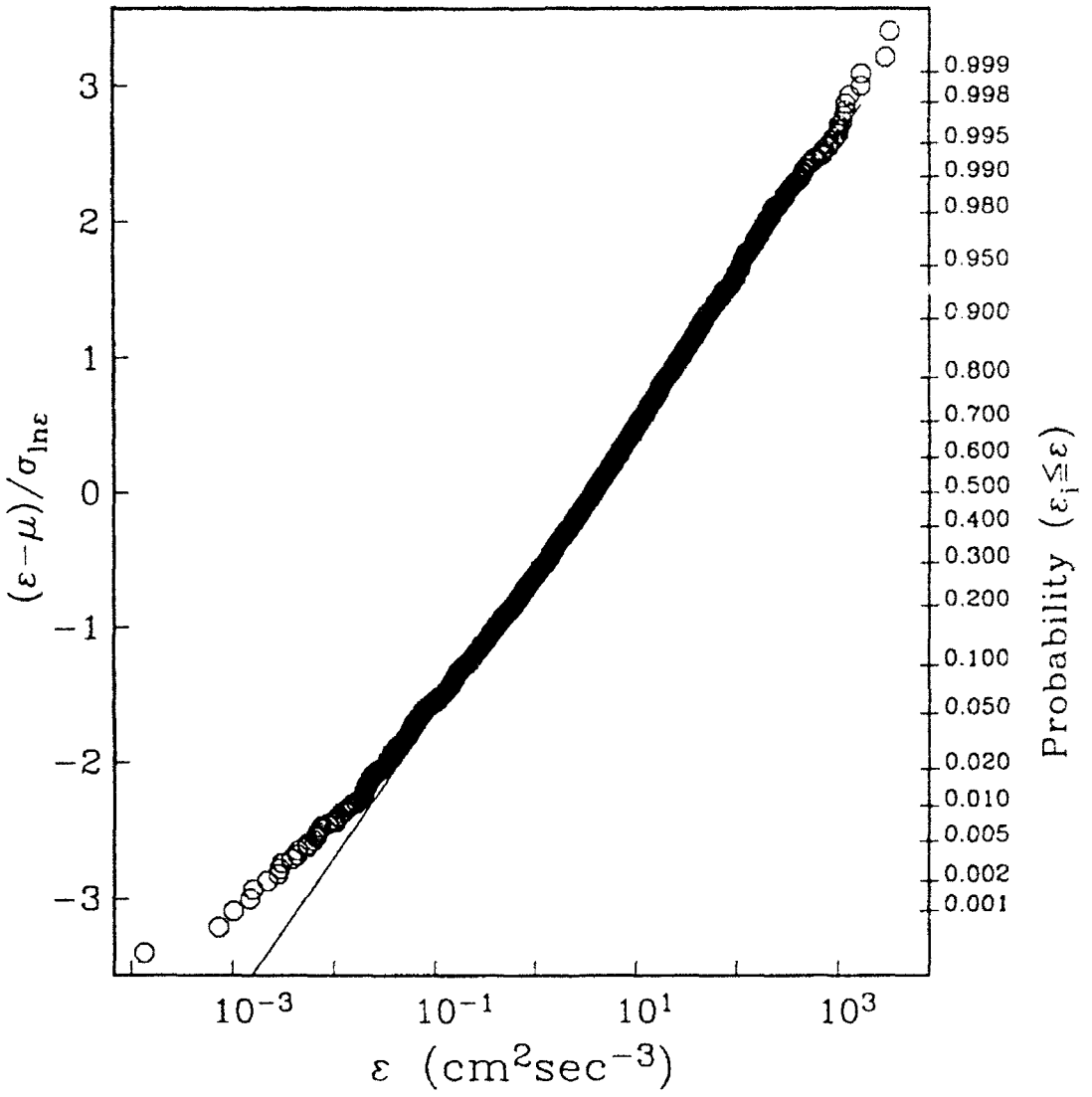

Figure 5. Dissipation rates (based on 1/8 s subsections of a 512 s record) plotted on semilog paper vs probability ($\varepsilon_i \leq \varepsilon$). The right ordinate is stretched so that data from a lognormal distribution lie on a straight line. The corresponding "standardized normal random variable" $(\varepsilon-\mu)/\sigma_{\ln\varepsilon}$ is shown on the left ordinate. A straight line (ideal lognormal distribution) is fit through the data. The inverse slope of the line is $\sigma_{\ln\varepsilon}$ and the zero-crossing is used to estimate μ.

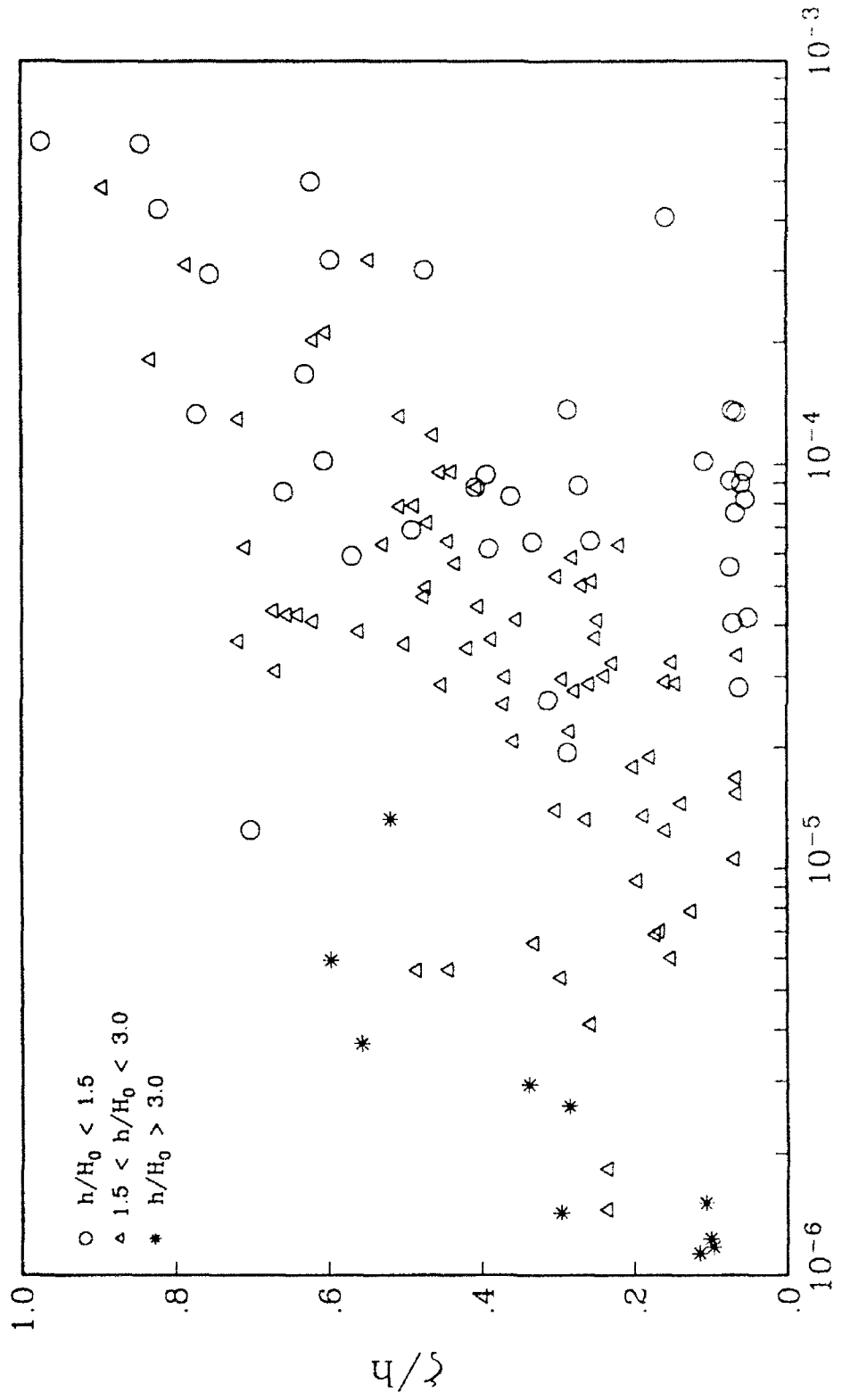

Figure 6. Dissipation rates vs relative water column position. Normalization is by u^3/l, using $(gh)^{1/2}$ for u and h for l. h is the local mean depth and H_0 is the significant waveheight in 7 m water depth.

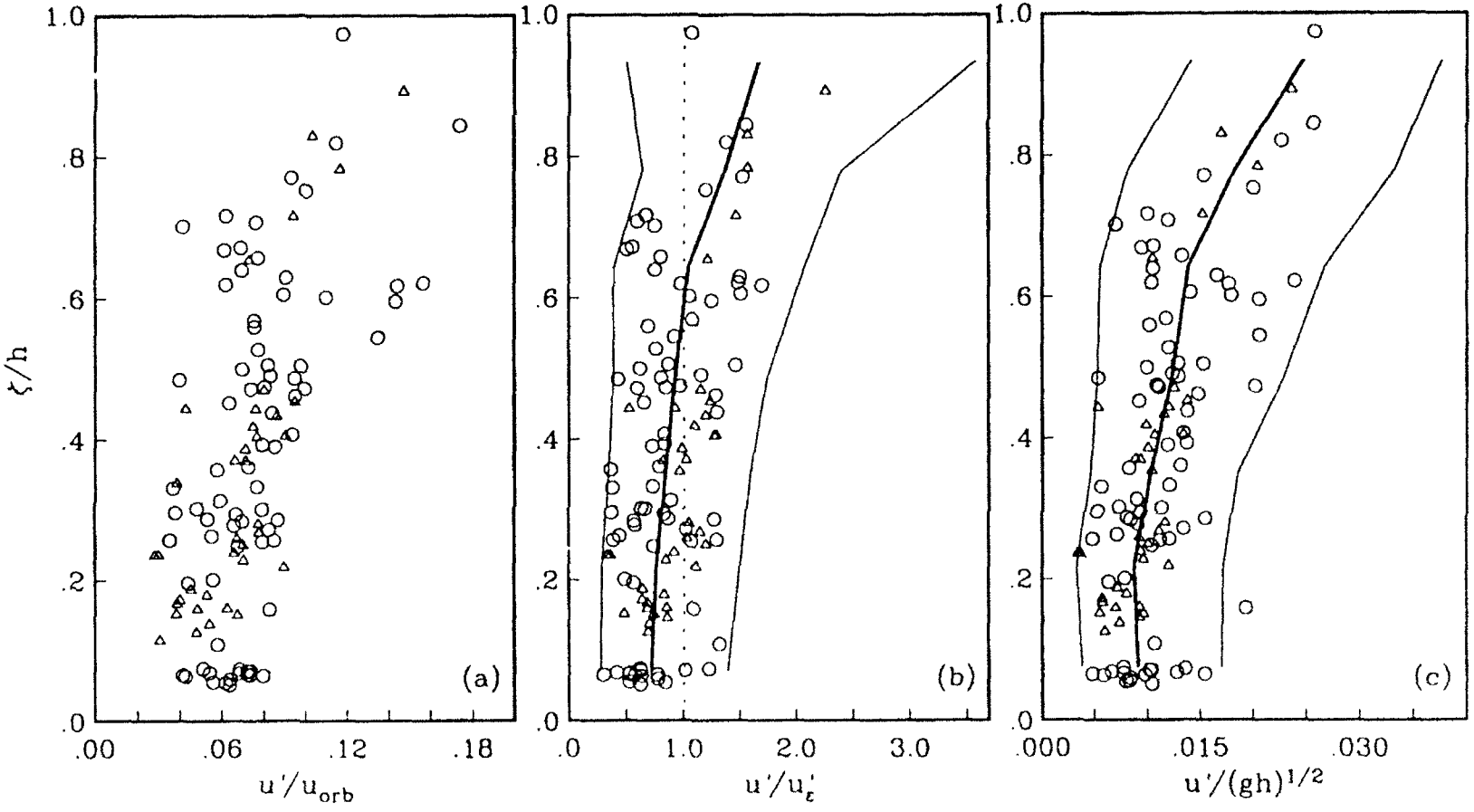

Figure 7. *Vertical profiles of turbulence intensity, u', for the 114 data points where* $h/H_0 < 3.0$. u' is normalized by (a) u_{orb}, the rms orbital wave velocity, (b) Equation (12), the bore dissipation model, and (c) $(gh)^{1/2}$, for comparison with laboratory data. In (b) and (c) the bold line connects mean u' values in seven vertical bins, while the lighter lines indicate ±1 standard deviation plus the uncertainty introduced at the data processing steps mentioned in the text.

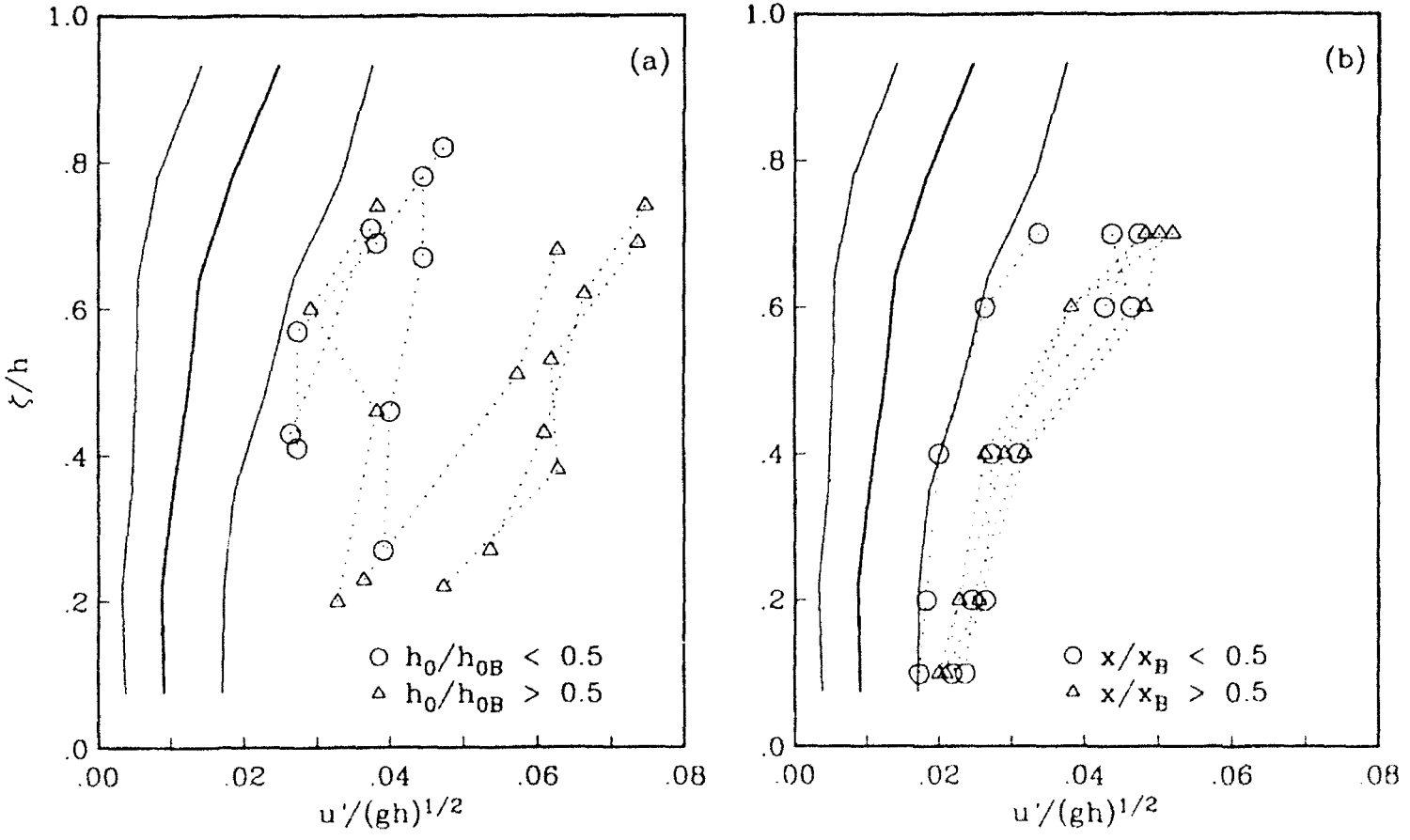

Figure 8. Vertical profiles of turbulence intensity, u′, scaled by $(gh)^{1/2}$. Field mean and bounds (solid lines) are from Figure 7(c). Laboratory results are from (a) Stive [1980] and (b) Hattori and Aono [1985]. The laboratory data are sorted by (a) h_0/h_{0L}, the ratio of local depth to breaking depth and (b) x/x_B, the ratio of distance from shore to surf zone width.

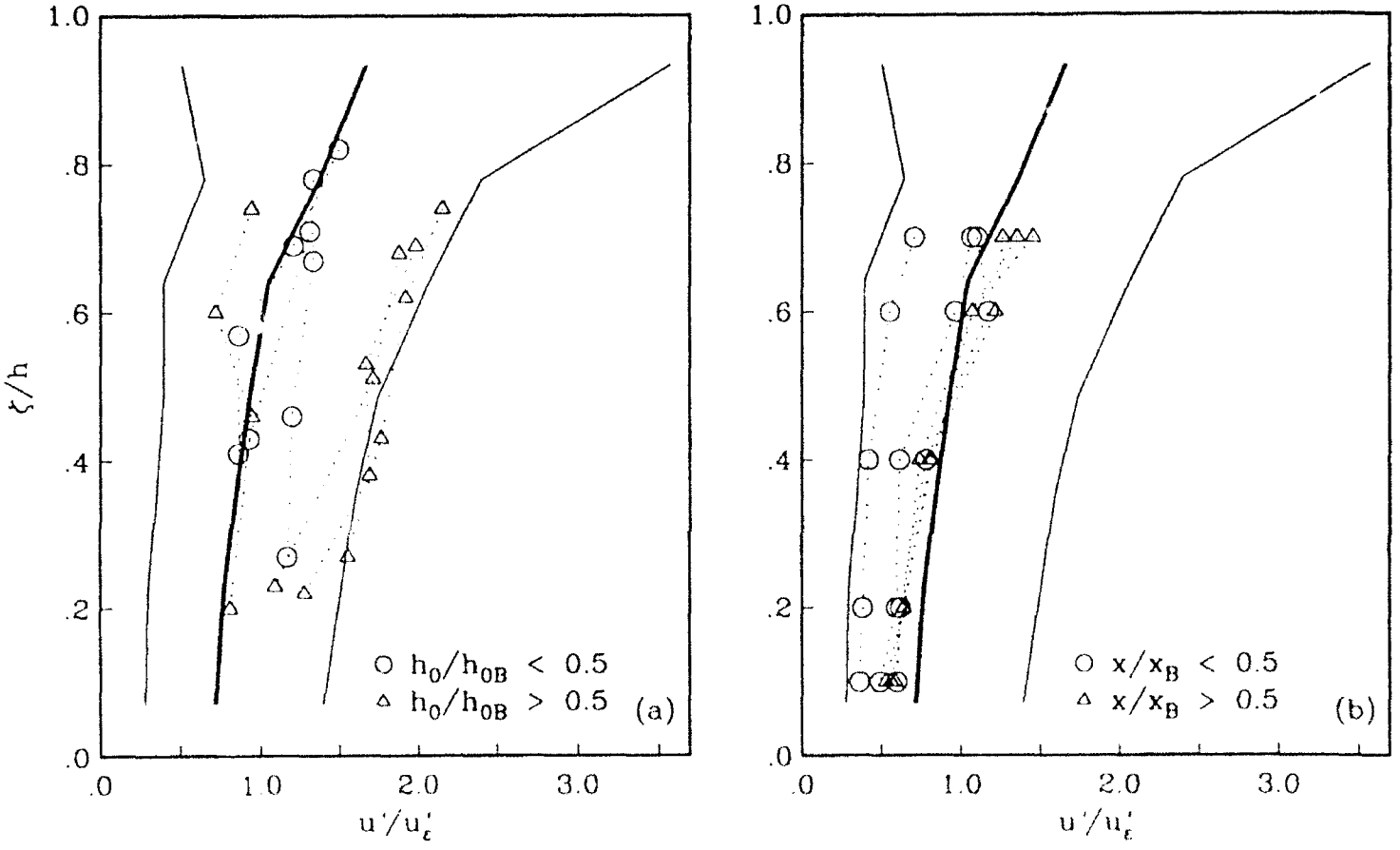

Figure 9. Vertical profiles of turbulence intensity, u′, scaled by u'/u'_ϵ (12). Field mean and bounds (solid lines) are from Figure 7(b). Laboratory data is from (a) Stive [1980] data and (b) Hattori and Aono [1985].

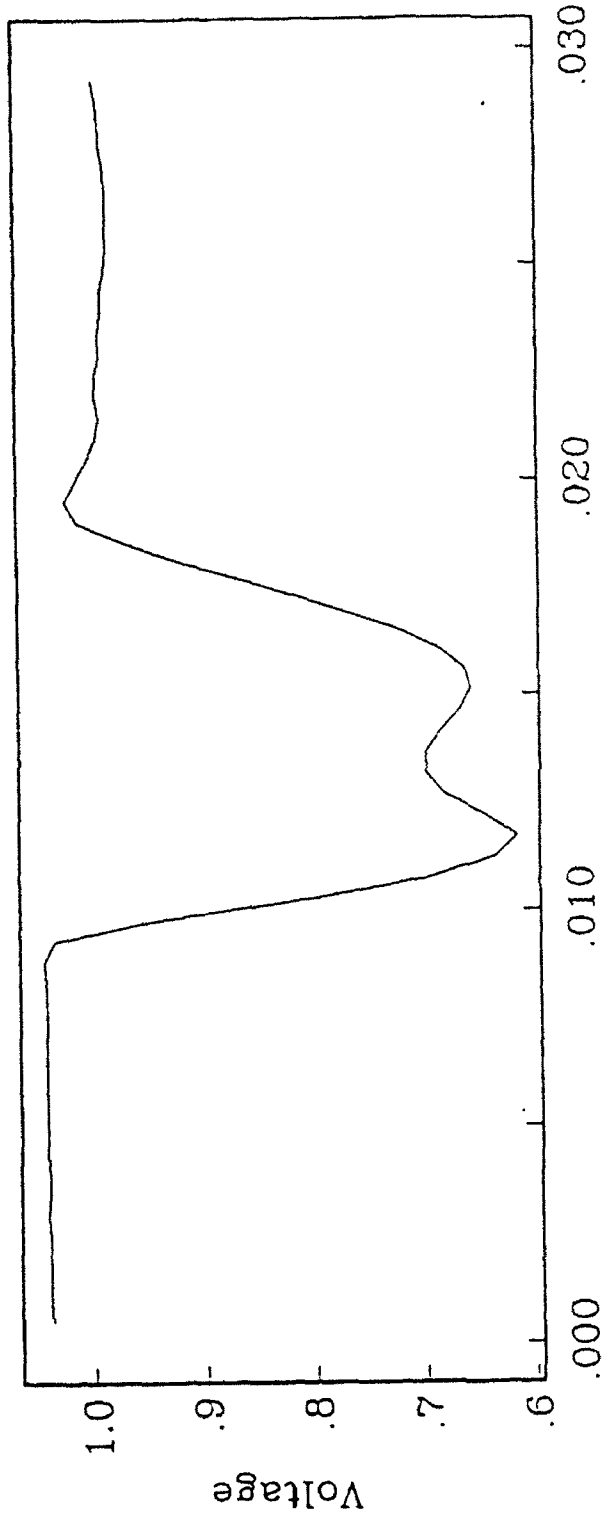

Figure A. Bubble signal in raw hotfilm voltage record.

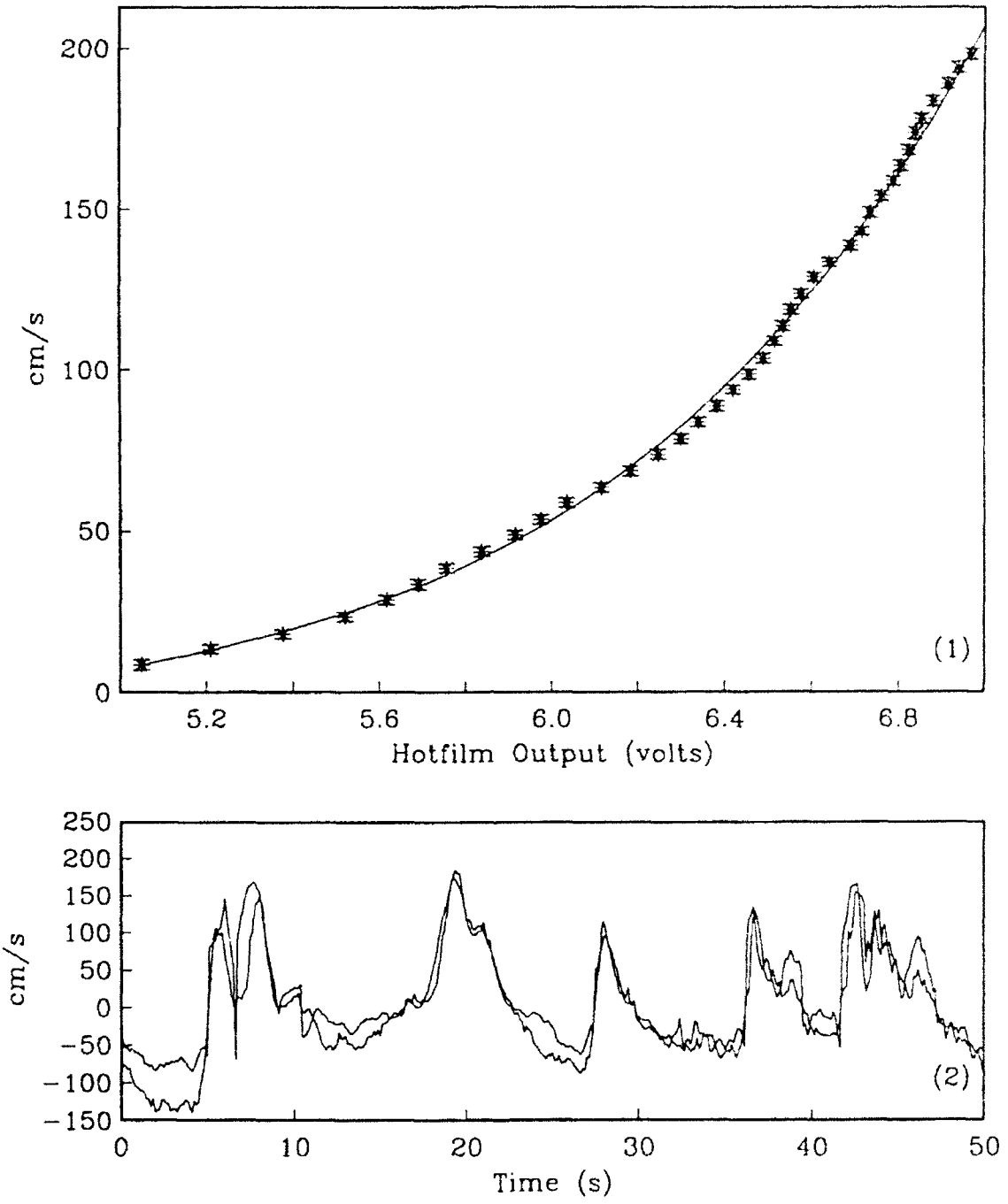

Figure B. (1) Typical hotfilm calibration curve. Error bars are ±1 standard deviation in each 5 cm/s bin. (2) Cross-shore velocity from the EM current meter and hotfilm (derectified to match the sign of the EM).

8. REFERENCES

Baker, M. A., and C. H. Gibson, Sampling turbulence in the stratified ocean: statistical consequences of strong intermittency, *J. Phys. Oceanogr., 17*, 1817-1836, 1987.

Battjes, J. A., Surf zone dynamics, *Ann. Rev. Fluid Mech., 20*, 257-293, 1988.

Battjes, J.A., and T. Sakai, Velocity field in a steady breaker, *J. Fluid Mech., 111*, 421-437, 1981.

Crawford, W. R., and T. R. Osborne, Microstructure measurements in the Atlantic equatorial undercurrent during GATE, *Deep-Sea Res., 26 (GATE Suppl. II)*, 285-308, 1980.

Delhaye, J. M., Hot-film anemometry in two-phase flow, *Proc. 11th National ASME/AIChE Heat Tx Conf.*, 58-68, 1969.

Flick, R. E., R. T. Guza, and D. L. Inman, Elevation and velocity measurements of laboratory shoaling waves, *J. Geophys. Res., 86*, 4149-4160, 1981.

Fuhrboter, A., Air entrainment and energy dissipation in breakers, *Proc. 12th Coastal Eng. Conf., 1*, 391-398, 1970.

Gibson, C. H., On the definition of turbulence, paper presented at International Workshop on Anisotropy of Fluid Flows in External Force Fields, and Geophysical, Technological, and Ecological Applications, Jurmala, USSR, Sept. 10-13, 1990.

Grant, H. L., R. W. Stewart, and A. Moilliet, Turbulence spectra from a tidal channel, *J. Fluid. Mech., 12*, 241-268, 1962.

Guza, R. T., M. C. Clifton, and F. Rezvani, Field intercomparisons of electromagnetic current meters, *J. Geophys. Res., 93 (C8)*, 9302-9314, 1988.

Hattori, M., and T. Aono, Experimental study on turbulence structures under spilling breakers, in *The Ocean Surface*, edited by Y. Toba and H. Mitsuyasa, pp. 419-424, D. Reidel, Hingham, Mass., 1985.

Hinze, J. O., *Turbulence*, 790 pp., McGraw-Hill, New York, New York, 1975.

Kolmogorov, A. N., A refinement of previous hypothesis concerning the local structure of turbulence in a viscous fluid for very large Reynolds number, *J. Fluid Mech.*, 13, 82-85, 1962.

Lin, C. C., On Taylor's hypothesis and the acceleration terms in the Navier-Stokes equations, *Quart. Appl. Math., 10*, 295, 1953.

Lumley, J. L., and E. A. Terray, Frequency spectra of frozen turbulence in a random wave field, *J. Phys. Oceanogr., 13*, 2000-2007, 1983.

Nadaoka, K., M. Hino, and Y. Koyano, Structure of the turbulent flow field under breaking waves in the surf zone, *J. Fluid Mech., 204*, 359-387, 1989.

Nadaoka, K., and T. Kondoh, Laboratory measurements of velocity field structure in the surf zone by LDV, *Coastal Engrg. in Japan, 25*, 125-145, 1982.

Nadaoka, K., T. Kondoh, and N. Tanaka, The structure of velocity field within the surf zone revealed by means of laser-doppler anemometry, *Rep. Port and Harbor Res. Inst., 21, No.2*, 49-106 (in Japanese), 1982.

Oboukhov, A. M., Some specific features of atmospheric turbulence, *J.Fluid Mech, 13*, 77-81, 1962.

Peregrine, D. H., and I. A. Svendsen, Spilling breakers, bores and hydraulic jumps, *Proc. 16th Int. Conf. Coastal Eng., 1*, 540-550, 1978.

Resch, F. J., and H. J. Leutheusser, Mesures des tensions de Reynolds dans le ressaut hydraulique, *J. Hyd. Res., 10*, 409-429, 1972.

Resch, F. J., H. J. Leutheusser, and S. Alemu, Bubbly two-phase flow in hydraulic jump, *J. Hyd. Div., 100*, 137-149, 1974.

Skjelbreia, J. E., Observations of breaking waves on sloping bottoms by use of laser doppler velocimetry, PhD. thesis, 176 pp., California Institute of Technology, Pasadena, May 1987.

Stive, M. J. F., Velocity and pressure field of spilling breakers, *Proc. 17th Int. Conf. Coastal Eng., 1*, 547-566, 1980.

Svendsen, I.A., Analysis of surfzone turbulence, *J. Geophys. Res., 92*, 5115-5124, 1987.

Thornton, E. B., Energetics of breaking waves within the surf zone, *J. Geophys. Res., 84*, 4931-4938, 1979.

Thornton, E. B., and R. T. Guza, Transformation of wave height distribution, *J. Geophys. Res., 88 (C10)*, 5925-5938, 1983.

Wang, S.L., Three-dimensional turbulence structure measurements in air/water two-phase flow, PhD. thesis, 442pp., Rensselaer Polytechnic, Troy, NY, August 1985.